CHARACTERIZING THE KINETICS OF LOCALIZATION AND ACTIVATION OF PI3K PARALOGS α AND β IN IMMUNE CELL SIGNALING

by

SARAH PEABODY

A THESIS

Presented to the Department of Chemistry & Biochemistry
and the Robert D. Clark Honors College
in partial fulfillment of the requirements for the degree of
Bachelor of Science

May 2023

An Abstract of the Thesis of

Sarah Peabody for the degree of Bachelor of Science
in the Department of Chemistry & Biochemistry to be taken June 2023

Title: Characterizing the Kinetics of Localization and Activation of PI3K Paralogs α and β in Immune Cell Signaling

Approved: *Scott D. Hansen Ph.D.*
Primary Thesis Advisor

Cell polarization and migration are critical processes performed by immune cells to execute their specialized functions. At the forefront of understanding these processes is the study of enzyme that catalyze biochemical reaction that drive immune cell activation. In particular, the rapid synthesis of the phosphatidylinositol (3,4,5)-trisphosphate ($PI(3,4,5)P_3$) is an early step in many immune cell signaling pathways. This reaction is catalyzed by phosphatidylinositol-3-kinase (PI3K) and a collection of membrane associated factors that controlling the localization and activity of PI3K. The proposed models in the field suggest that the activity of PI3K paralogs α and β are controlled through synergistic binding of a variety of membrane proteins including GβGγ, pY peptides, and the Rho-family small GTPases Rac1 or HRas. However, these previous studies have not addressed which of these factors control PI3K localization to membranes and which play a role in directly activating the enzyme. For my thesis, I used supported lipid bilayer technology and Total Internal Reflection Fluorescence (TIRF) microscopy to study how different PI3K regulatory factors drive the localization or activation of PI3Kα and PI3Kβ. Using these techniques, I was able to determine that both PI3Kα and β are primarily localized to membranes by RTK derived phosphorylated tyrosines (pY) peptides. Once bound to pY peptide, PI3Kα and β can form secondary interactions with either HRas for PI3Kα or Rac1/GβGγ for PI3Kβ. These

secondary interactions can enhance membrane binding dynamics of PI3K, but they are unable to drive localization on their own, and instead must work in tandem with pY peptides. Finally, I found that activation of PI3Kα and β by the combination of inputs is not proportional to the change in localization, suggesting that synergistic activation of PI3K is driven by an allosteric mechanism.

Acknowledgements

There are so many people that go into making a project like this possible, from the people that are in the room where the science happens to those who have supported me throughout my college years and beyond.

To Professor Scott Hansen and PhD student Benjamin Duewell, thank you for your constant support and feedback. This project does not exist without their endless hours of experiments, analysis, and editing. I am so grateful for the time and energy they have put into mentoring me as both a student and a scientist. Additionally I would like to thank the rest of the members of the Hansen Lab, I would not have enjoyed my time working as an undergraduate researcher nearly as much without them.

To my honors college thesis advisor, Lindsay Hinkle, thank you for all the time and energy you have put into your feedback and advice.

To my friends. I am so lucky to have had the best support system through my four years of undergraduate studies, and I would never have survived the long days and late nights, intense frustration, and the many failures along the way without them.

And lastly, but most importantly, to my parents and my sister for their unwavering belief in me and their endless support. Thank you for being my role models, mentors, and number one fans.

Table of Contents

Introduction 7

Results 15

Validation of the PI(3,4,5)P_3 sensor, Btk. 15

PI3Kβ localization is mediated by pY peptides, Rac1, and GβGγ. 19

Active Rac1 and GβGγ work synergistically with pY to activate PI3Kβ. 23

PI3Kα localization is mediated by pY peptides and HRas. 25

Active HRas works synergistically with pY to activate PI3Kα. 28

Discussion 30

Methods 34

Bibliography 41

List of Figures

Figure 1. PI3K signaling inputs and function. 10
Figure 2. *In vitro* methods for visualizing PI3K localization 12
Figure 3. Hypothesized model for binding dynamics of PI3K Paralogs α and β. 14
Figure 4. Btk acts as an alternative PI(3,4,5)P3 sensor to Grp1. 18
Figure 5. PI3Kβ localization is mediated by pY peptides, Rac1, and GβGγ. 22
Figure 6. Active Rac1 and GβGγ work synergistically with pY to activate PI3Kβ. 25
Figure 7. PI3Kα localization is mediated by pY peptides and HRas. 28
Figure 8. Active HRas works synergistically with pY to activate PI3Kα. 29

Introduction

Immune cells respond to chemical cues in their environment, which are essential for targeting and destroying invading pathogens. Cell signaling in immune cells requires communication between cell receptors and peripheral membrane proteins on the intracellular plasma membrane. The inner leaflet of the membrane in eukaryotic membrane-enclosed organelles is composed of different kinds of phosphatidylinositol phosphate (PIP) lipids that exist in different concentrations in various regions of the cell. At the plasma membrane, phosphatidylinositol 3,4,5-trisphosphate ($PI(3,4,5)P_3$) plays a critical role in driving cell signaling, polarization, and migration (DiPaolo, 2006). $PI(3,4,5)P_3$ was first discovered in 1988 in neutrophilic white blood cells (neutrophils) (Whitman, 1988). Given its high negative charge, $PI(3,4,5)P_3$ is thought to be involved in anchoring membrane proteins and controlling membrane cytoskeleton interactions (Hammond, 2012). The lipid was also hypothesized to be physiologically relevant due to its transient nature at the plasma membrane (Traynor-Kaplan, 1988), and researchers found that $PI(3,4,5)P_3$ levels increased 40-fold directly following its activation (Stephens, 1991). This synthesis of $PI(3,4,5)P_3$ is now known to be a highly regulated process performed by the phosphoinositide 3-kinase (PI3K) family of enzymes. PI3Ks are a widely important intracellular lipid generator in cell biology. In neutrophils, PI3K activation and, in turn, $PI(3,4,5)P_3$ synthesis is responsible for controlling the activity of many downstream proteins that regulate important aspects of cell function, including cell proliferation and immune cell migration (Stephens, 1993). PI3K is the second most mutated protein in cancer and as such PI3K inhibitors have become a popular drug target in recent years (Nussinov, 2021; Vanhaesebroeck, 2012).

The PI3K Class I family consists of three paralogs, α, β, δ, and γ, and each serves different roles in the regulation of cell functions (Vanhaesebroeck, 1997). Given the non-redundant roles of the four paralogs (Vanhaesebroeck, 2010), understanding the differences in the kinetics of activity in each paralog is important to being able to design drug therapies that target specific cell signaling functions. We chose to focus on PI3K paralogs α and β because they both associate with phosphorylated tyrosine (pY) peptides but are synergistically activated by different regulatory factors. By contrast, PI3Kγ does not interact with pY peptide and is directly activated by membrane anchors heterotrimeric G-protein, GβGγ.

PI3Kα and β are engaged downstream of receptor tyrosine kinases (RTKs) via binding of the p85 regulatory subunit by their SH2 domains with pY peptides. These tyrosine residues are auto phosphorylated upon dimerization of receptor tyrosine kinases (RTKs), leading to an increase in PI3K activity above basal level (Rameh, 1995; Houslay, 2016; Lee, 2011). Both paralogs also contain a conserved Ras/Rho binding domain (RBD) capable of binding to specific small GTPases and stimulating activity (Rodriguez-Viciana, 1996). Small GTPases are signaling proteins that are spatiotemporally activated and serve as molecular scaffolds to recruit other proteins to them during cell response to a stimulus, quickly triggering the desired response (Olayioye, 2019). Without small GTPase activity, a slow response or non-responsive state is observed. Small GTPases turn PI3K “ON” by binding to guanosine triphosphate (GTP), transitioning PI3K to its active conformation. When the small GTPase binds guanosine diphosphate (GDP), it dissociates from PI3K, transitioning the kinase to its “OFF” or inactivate state (Worthylake, 2000). PI3Kβ preferentially binds to Rac family small GTPase 1 (Rac1), while PI3Kα binds preferentially to the GTPase HRas, from "Harvey Rat sarcoma virus"

(Fritsch, 2013; Rodriguez-Viciana, 1994; Buckles, 2017). Additionally, the PI3Kβ paralog has another small molecule hypothesized to be involved in its kinetic activity, the heterotrimeric G-proteins, GβGγ (Thomason, 1994). GβGγ is activated downstream of G-protein coupled receptors (GPCRs) (Hamm, 1998). GPCRs provoke cellular responses, regulating many cellular functions by coupling to G-proteins, which transduce the incoming signal into the cell. GβGγ subunits are membrane anchored proteins that have been shown to directly interact with the catalytic subunits of PI3K (Maier, 2000). (**Figure 1**)

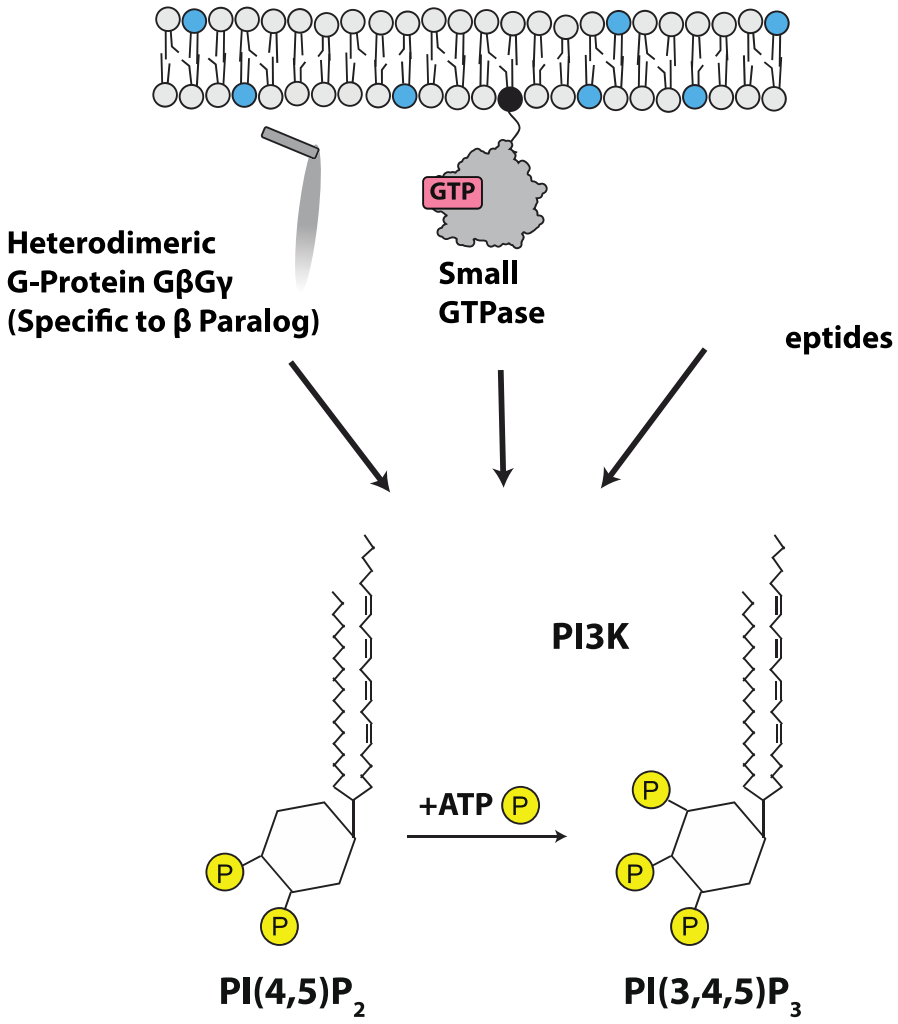

Figure 1. PI3K signaling inputs and function.

Graphical depiction of the PI3K signaling inputs Heterodimeric G-Proteins GβGγ, active (GTP bound) Small GTPases, and Receptor Tyrosine Kinase (RTK) associated Phosphorylated Tyrosine (pY) Peptides. All these signaling inputs lead to activity of PI3K, which catalyzes the conversion of $PI(4,5)P_2$ to $PI(3,4,5)P_3$ using a phosphorous group from ATP.

We hypothesize that the activity of PI3K at the plasma membrane is regulated by two mechanisms. The enzyme must be targeted to the plasma membrane in a process called

localization, and then the enzyme must be turned on in a process called activation. Historically, the field of biochemistry and molecular biology has studied PI3K using low resolution kinetic assays performed in solution that lack the complexity of the plasma membrane environment. Although these studies have shown what molecules are necessary for catalytic activity of PI3K, they have not been able to decipher how various factors control localization verses activation. Previously, it was shown that the activity of the p110α and β catalytic subunits decreases when the p85 regulatory subunit is coexpressed in cells, suggesting that PI3Kα and β may be autoinhibited (Yu, 1998). When RTKs' pY peptides compete with the p110 catalytic subunit to bind the nSH2/cSH2 domains of the p85 regulatory subunit, the autoinhibitory contacts are released, and PI3K activity increases dramatically (Nolte, 1996; Hon, 2011). We hypothesize that pY-membrane binding is the critical first step of PI3K activation in the α and β paralogs, relieving PI3K autoinhibition and allowing for further binding to other membrane anchored proteins. Previous studies have utilized pY peptides in solution, however, this is not the physiologically relevant configuration. To address this limitation of previous work, we covalently attached our pY peptides directly to supported lipid bilayers (SLBs). These are synthetic membranes designed to mimic the plasma membrane and can be created using different lipid compositions to test for specific interactions that are hypothesized to regulate PI3K localization and activity. In order to visualize the activity of PI3K on our SLBs, we used Total Internal Reflection Fluorescence (TIRF) microscopy, a form of microscopy used to reduce background noise and focus specifically on proteins on or near a membrane surface. We use two different visualization methods, one for measuring PI3K localization and one for measuring PI3K activation. To visualize localization of PI3K, we chemically labeled the kinase in a site-specific manner using a fluorescent dye (**Figure 2**). To visualize PI3K activation, we measured

PI(3,4,5)P_3 production using a fluorescent biosensor that binds specifically to PI(3,4,5)P_3's phospholipid head.

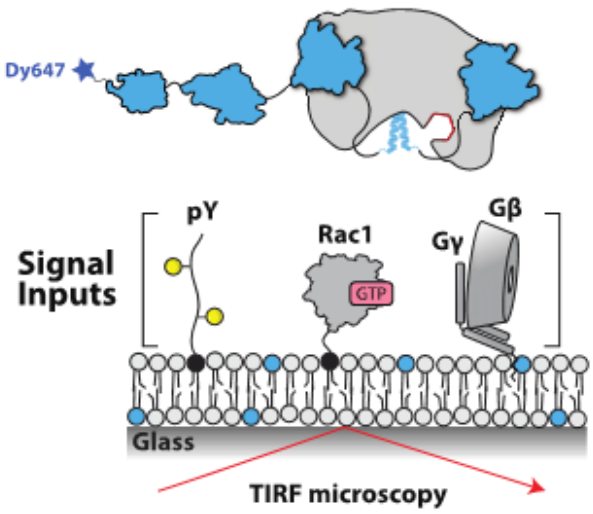

Figure 2. *In vitro* methods for visualizing PI3K localization

PI3K recruitment to supported lipid bilayers is visualized using total internal reflection fluorescence (TIRF) microscopy. Supported lipids bilayers are composed of DOPC, MCC, and PIP_2 lipids.

For a biosensor to be effective, it must bind specifically to the target protein and not interfere with other protein interactions in the experimental system. In addition, the biosensor should display rapid association and dissociation kinetics when interacting with the target protein. There are a number of PI(3,4,5)P_3 specific PH domains that are currently available for use as biosensors (Pilling, 2011). Among them are, general receptor for phosphoinositides 1 (Grp1) and Bruton's Tyrosine Kinase (Btk). While Grp1 is more commonly used as a PI3K fluorescent biosensor, both biosensors can be used to visualize the abundance and spatial distribution of PI(3,4,5)P_3 lipids created downstream of PI3K. While Grp1 is a specific biosensor

for $PI(3,4,5)P_3$ lipids, our lab has found that it is not an ideal sensor due to the fact that we suspect it is able to bind two $PI(3,4,5)P_3$ phospholipid heads. This results in more complex reaction kinetics that are not necessarily reflective of the kinetics of the lipid kinase. Ideally, our $PI(3,4,5)P_3$ biosensor would only be able to bind one phospholipid head per one biosensor molecule.

Bruton's tyrosine kinase (Btk) is a cytoplasmic tyrosine kinase involved in B cell signal transmission that has been shown to be activated only after being localized to the plasma membrane by $PI(3,4,5)P_3$ (Hendricks, 2014). Btk has been used in multiple published papers as a measure of $PI(3,4,5)P_3$ production, including the work done by the Jean Chung lab (Chung, 2019) who provided us with our Btk construct plasmid. Similarly to Grp1, Btk binds phospholipid heads of $PI(3,4,5)P_3$ via its PH domain, but we have mutated our Btk construct to only bind one phospholipid head. As a result, we expect to see more easily interpretable kinetics data using the Btk biosensor.

Purification and characterization of the Btk sensor was the first step toward reaching my goal of measuring the kinetics of PI3Kα/β localization and activity. In order to understand the activation and localization of PI3K, we must be able to distinguish between the kinetics of PI3K under different conditions, requiring biosensors that produce accurate and reproducible data. Using a combination of biosensors and fluorescently labeled proteins, we will look at the kinetics of each small molecule involved in localization and activation of each of these two paralogs. Our new k_{cat} values can be used to measure changes in PI3K catalytic activity with the addition or removal of supporting molecules. This kinetic data will allow us to determine which membrane

tethered regulatory proteins are involved in activation, which are involved in localization, and which might be involved in both (**Figure 3**). Using a combination of SLBs with TIRF microscopy experiments, we will visualize the effects of GβGγ subunits, Rac1, and pY in the β paralog, and HRas and pY in the α paralog.

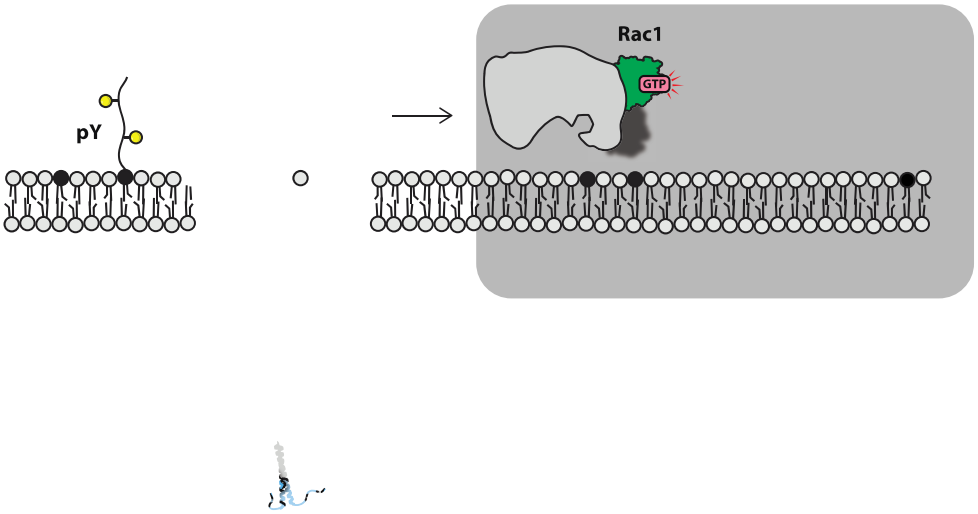

Figure 3. Hypothesized model for binding dynamics of PI3K Paralogs α and β.

First, PI3K autoinhibition is relieved by binding of a pY peptide, then secondary interactions with small GTPases and GβGγ can enhance the membrane binding dynamics of PI3K.

Through an assortment of bulk activity assays and single molecule data we conclude that pY is necessary for the localization of both PI3Kα and β, and small GTPases, and in PI3Kβ GβGγ, work synergistically with pY to synergistically activate these PI3K paralogs.

Results

Validation of the PI(3,4,5)P_3 sensor, Btk.

Our previous experiments measuring production of PI(3,4,5)P_3 on supported lipid bilayers using Grp1 have shown an accumulation of molecules on the sensor, potentially due to this biosensor being able to bind two phospholipid heads. This accumulation causes the fluorescence intensity measured to continue to increase even after the reaction has gone to completion, leading us to search for a new biosensor. Before beginning our larger goal of characterizing PI3K kinetics, we tested the potential of Btk as an alternative biosensor. For a biosensor to be effective, it must have a fluorescent tag for visualization. Fluorescent tags come in many different forms, but the most common variation is a fluorescent protein built into the plasmid construct. Fluorescent proteins exhibit fluorescence when exposed to light in a certain range of wavelengths when aromatic side chains phenylalanine, tyrosine, or tryptophan are excited (Springer, 2000). While fluorescent proteins are convenient and easy to use, they also have some downsides including being relatively large, which can sterically hinder the function of small proteins. They are also less versatile because they are single color because on the genetically encoded sequence. For my research, I used the SNAP tag fusion protein which can be chemically labeled with fluorophores derivatized with a benzyl guanine chemical (Erdmann, 2019). Compared to fluorescent proteins, the SNAP tag dyes have a higher fluorescence quantum yield , slower photobleaching kinetics, and can be versatilely labeled with different colored dyes, thus increasing the flexibility of our experiments (Cole, 2014). Since the construct acquired from the Chung Lab at Colorado State was tagged with a green fluorescent protein (eGFP), I first used molecular cloning techniques to design a plasmid construct with a SNAP-tag construct in place

of the fluorescent protein. Then, I recombinantly expressed the SNAP-tagged Btk and measured its specificity for $PI(3,4,5)P_3$ lipids.

We first confirmed the specificity of Btk-SNAP-Ax488 (Btk-Ax488) for $PI(3,4,5)P_3$ over $PI(4,5)P_2$ on supported lipid bilayers (SLBs) using Total Internal Reflection Fluorescence (TIRF) Microscopy (**Figure 4A**). Still images show minimal binding of Grp1-Ax555 or Btk-Ax488 to a 98% DOPC, 2% $PI(4,5)P_2$ membrane, but strong binding of both Grp1-Ax555 and Btk-Ax488 to a 98% DOPC, 2% $PI(3,4,5)P_3$ membrane. We can thus confirm the specificity of both of these biosensors for $PI(3,4,5)P_3$ lipids.

To confirm the binding of $PI(3,4,5)P_3$ to Btk and visualize this binding, previous x-ray crystallography research has produced a structure of the Btk PH domain in complex with inositol (1,3,4,5)-tetrakisphosphate ($Ins(1,3,4,5)P_4$) (Baraldi, 1999). $Ins(1,3,4,5)P_4$ and $PI(3,4,5)P_3$ bind to Btk in the same interactions, but $Ins(1,3,4,5)P_4$ is easier to crystalize than the more complex $PI(3,4,5)P_3$. The crystal structure solved by Baraldi et al. shows the PH domain of the Btk protein in blue and the phospholipid head of $Ins(1,3,4,5)P_4$ in its spherical form bound to the construct (**Figure 4B**).

We measured the bulk recruitment of each biosensor to a 98% DOPC, 2% $PI(3,4,5)P_3$ SLB membrane by using TIRF-M to visualize the intensity of the Grp1-Ax555 and Btk-Ax488 fluorescence over time. As opposed to our previously collected data, where Grp1-Ax555 fluorescence intensity never reaches a plateau, when using the Btk-Ax488 biosensor we see a clear plateau in the fluorescence intensity when the reaction is complete (**Figure 4C**).

In order to see if the two biosensors show differences in membrane binding behavior, we visualized single molecule binding events to measure three properties: diffusion, dwell time, and on rate of each biosensor. We study diffusion to make suggestions about how molecules are bound to the membrane. To do so, we find the probability of each experimental group traveling a certain distance across the membrane over each camera frame. This distance travelled is described as the step size. If a molecule is held in place on the membrane by one tether point, it will have more flexibility to move than a molecule that is held at two tether points. This can allow us to better understand the binding kinetics of proteins on the membrane. If PI3Kβ can bind two pY peptides, we would expect to see this phenomena (of more PI3Kβ molecules bound to two pY peptides) occur more frequently as the concentration increases, since the pY peptides will become more closely packed on the membrane. This would lead to a characteristically slower moving group of doubly tethered molecules. If we do not see this slower moving group of molecules, we suggest that each PI3Kbeta only binds one pY peptide. Since we see no significant difference between the diffusions of the two biosensors, we suggest that both biosensors bind the same number of phospholipid head groups, assumed by our construct mutation to be one (**Figure 4D**). Dwell time measures the time a fluorescent molecule remains on the membrane between binding and leaving. In our experiments, we see that the dwell time of the Grp1-Ax555 biosensor (τ_1=0.383 s, τ_2=0.945 s) is significantly longer than the dwell time of Btk-Ax488 (τ_1=0.197 s, τ_2=0.2004 s) (**Figure 4E**). Additionally, we see a greater number of cumulative binding events per second for the Btk-Ax488 biosensor than Grp1-Ax555, leading to a greater on rate for the Btk-Ax488 biosensor (k_{on}=2.51 molecules/nm•μm^2•sec) than Grp1-Ax555 (k_{on}=0.69 molecules/nm•μm^2•sec) (**Figure 4F**). Put together, this single molecule data

tells us that the Btk-Ax488 biosensor binds PI(3,4,5)P_3 more efficiently but doesn't dwell as long as Grp1-Ax555, leading Btk to be an effective alternative PI(3,4,5)P_3 sensor to Grp1.

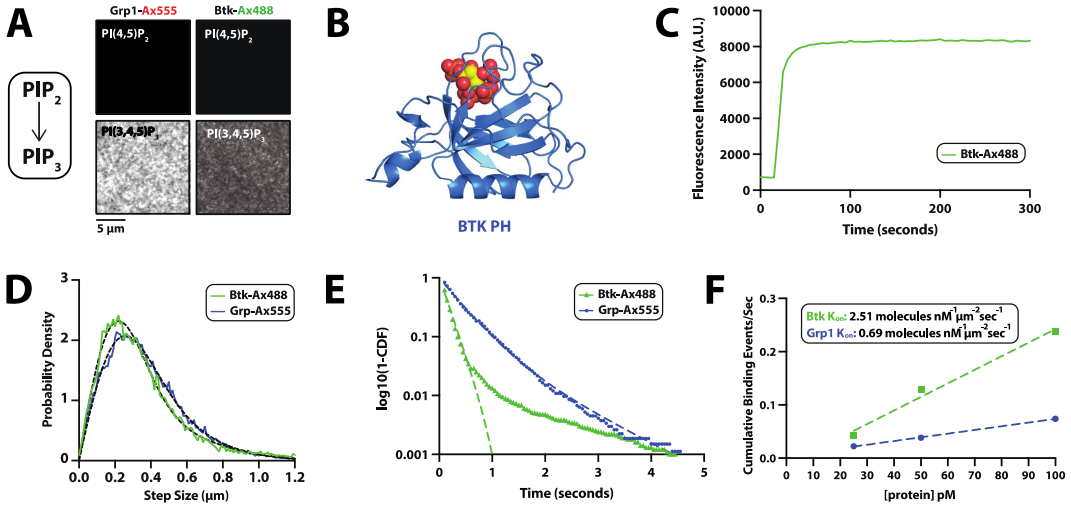

Figure 4. Btk acts as an alternative PI(3,4,5)P3 sensor to Grp1.

(A) Representative TIRF-M images showing the localization of 50 nM Grp1-Ax555 and 50 nM Btk-SNAP-Ax488 on supported lipid bilayers containing 2% PI(4,5)P_2 or 2% PI(3,4,5)P3, plus 98% DOPC. (B) Crystal structure of Btk PH domain binding to Ins(1,3,4,5)P_4. X-ray crystal structure determined by Baraldi et al. (Baraldi, 1999) (BTK, E41, PDB 1B55). (C) Bulk membrane absorption kinetics for 10 nM Btk-Ax488 and Grp1-Ax555 measured on membrane containing PI(3,4,5)P_3. Membrane composition: 98% DOPC, 2% PI(3,4,5)P_3. (D) Representative step-size distributions measured in the presence of either 50 pM Grp1-Ax555 or 50 pM Btk-Ax488. (E) Single molecule dwell time distributions measured in the presence of 50 pM Btk-Ax488 or 50 pM Grp1-Ax555. (F) Binding frequency calculated from cumulative number of binding events seen at 25pM, 50pM, and 100pM Btk-Ax488 or Grp1-Ax555. The slopes from the cumulative membrane binding events were plotted against the concentration of Grp1-Ax555 and Btk-Ax488 to calculate the following association rate constants: k_{on}(Grp1-Ax555) = 0.69 Grp1 nM^{-1} μm^{-2} sec^{-1}; k_{on}(Btk-Ax488): 2.51 molecules nM^{-1} μm^{-2} sec^{-1}. Membrane composition for single molecule measurements: 98% DOPC, 2% PI(3,4,5)P_3.

PI3Kβ localization is mediated by pY peptides, Rac1, and GβGγ.

Studies done previously in the literature have shown pY peptides, Rac1 GTPase, and GβGγ to be involved in the activity of PI3Kβ (Houslay, 2016, Worthylake, 2000, Maier, 2000). To determine how these membrane tethered proteins regulate localization of PI3Kβ, we used fluorescent sensors to detect PI3Kβ at the membrane in the presence of our membrane anchored proteins of interest.

Given that pY peptides are membrane bound in the cell, we hypothesized that at a single molecule concentration regime of Dy647-PI3Kβ (~10pM) we would see variation in the levels of recruitment of the fluorescently labeled Dy647-PI3Kβ between a sample with no pY peptides present, pY peptides in solution, and pY peptides membrane tethered. For the membrane tethered pY peptides, we covalently attached pY peptides to supported membranes using cysteine reactive maleimide lipids. A still image was captured of each sample (no input, pY in solution, and membrane tethered pY) for comparison. Consistent with our hypothesis, we see little to no binding in both the no input and pY in solution images, while in the pY tethered we see a significant increase in binding of Dy647-PI3Kβ (**Figure 5A**). This suggests that membrane bound pY is able to localize Dy647-PI3Kβ and is more effective at recruiting it than pY in solution.

We follow this up by exploring if this localization of Dy647-PI3Kβ by pY is concentration dependent by increasing the density of pY peptides tethered to the membrane. As the concentration of pY peptide tethered to the membrane increases, we observed an increase in the density of membrane bound Dy647-PI3Kβ (**Figure 5B**). This tells us that recruitment of

Dy647-PI3Kβ has a positive correlation to pY peptide concentration. If this positive correlation was due to Dy647-PI3Kβ being able to bind more pY peptides at higher concentrations of pY, we would expect to see a significant difference in the step-size diffusion of the three samples at varying concentration. Instead, we see similar diffusions between the three sample groups (**Figure 5C**), suggesting that this concentration dependent increase in localization is not due to one Dy647-PI3Kβ being bound multiple times, but due to more pY peptides being bound to Dy647-PI3Kβ at the membrane.

To determine the impacts of the addition of small GTPase Rac1 on the activity of Dy647-PI3Kβ, we membrane tethered recombinantly purified Rac1 to the membrane by the same process as the pY peptides. Just as we had seen previously, pY peptides show localization of Dy647-PI3Kβ without any additional small molecules. However, upon the addition of small GTPase Rac1, the membrane intensity of Dy647-PI3Kβ increases, showing synergistic localization by the two small molecules (**Figure 5D**). We see a distinct difference in the step size diffusion populations between the experiment with just pY and the pY+Rac1(GTP) experiment (**Figure 5E**), telling us that this increase in localization is due to one Dy647-PI3Kβ molecule binding both a pY peptide and a Rac1, decreasing its ability to diffuse across the membrane.

The last regulatory factor shown to be involved in the activity of PI3Kβ is the heterodimeric G-protein GβGγ (Thomason, 1994). To determine how GβGγ impacts PI3Kβ localization, we performed two different experiments with GβGγ and compared them against a control membrane with only tethered pY. As previously described, pY peptides tethered to the membrane are sufficient for PI3Kβ recruitment. When farnesyl GβGγ is passively absorbed into

the supported membrane in addition to the tethered pY, we see a two-fold increase in localization of Dy647-PI3Kβ. This tells us that GβGγ and pY act synergistically to localize Dy647-PI3Kβ to the membrane. In our third experiment, we see that when pY peptides are in solution and GβGγ is passively absorbed into the membrane, there is no localization of Dy647-PI3Kβ (**Figure 5F**). This tells us that without tethered pY peptides, GβGγ alone is unable to localize Dy647-PI3Kβ, but when tethered pY peptides are present at the membrane, it is able to support localization. To determine whether this synergy is due to GβGγ and pY jointly binding Dy647-PI3Kβ, we measured the step size diffusion of the pY tethered Dy647-PI3Kβ and the pY tethered with GβGγ-Dy647-PI3Kβ. Just as we saw with Rac1, there are two distinct populations in the step size diffusions (**Figure 5G**), suggesting to us that the increase we see in localization is due to a GβGγ and a tethered pY both binding one PI3Kβ, once again decreasing its ability to diffuse across the membrane.

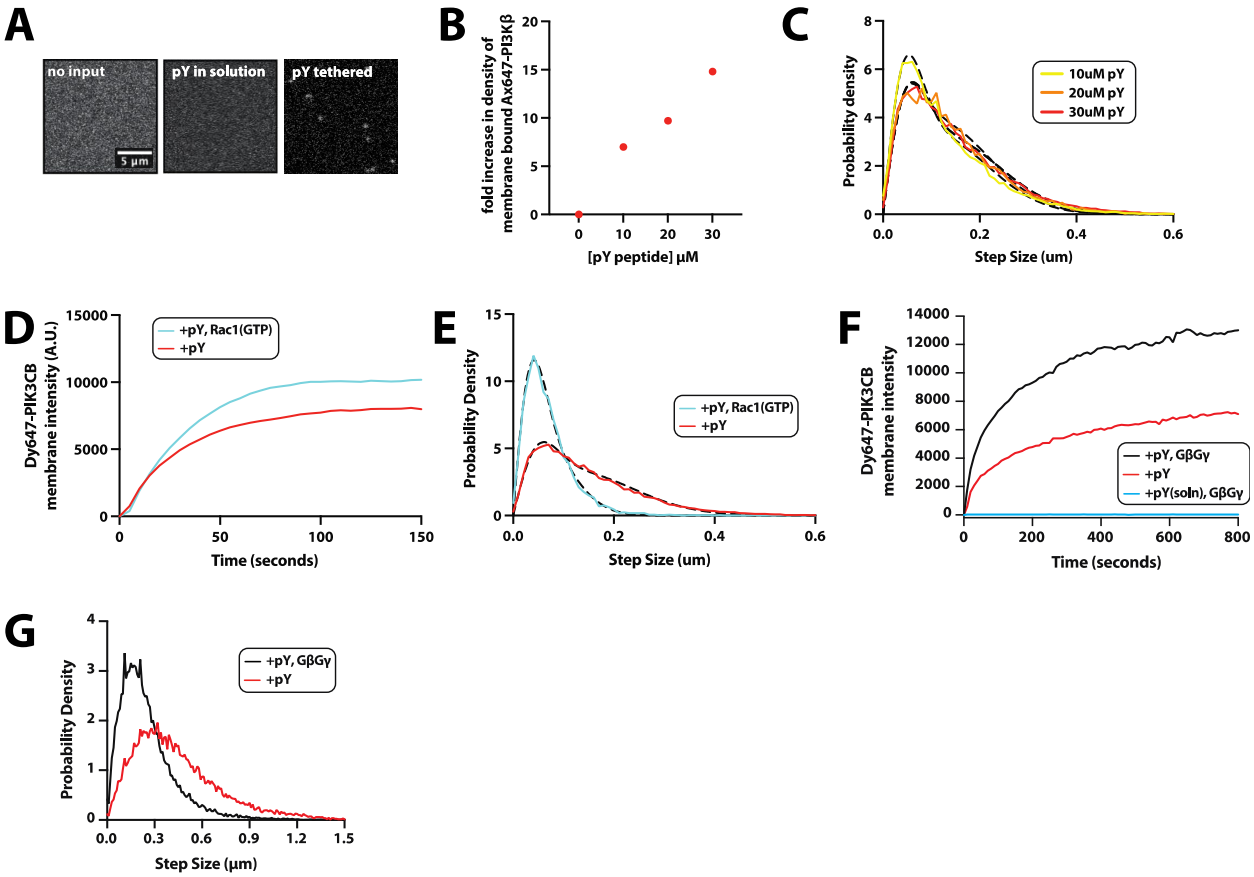

Figure 5. PI3Kβ localization is mediated by pY peptides, Rac1, and GβGγ.

(A) Representative TIRF-M images showing the membrane localization of 5-10 pM Dy647-PI3Kβ on membranes containing either no inputs, pY(solution), or pY(tethered). Supported membrane for pY tethered was conjugated with 10 µM pY peptide before adding Dy647-PI3Kβ. pY(solution) = 10 µM. (B) Relationship between the total pY solution concentration (x-axis) used for covalent conjugation and the fold increase in density of membrane bound Dy647-PI3KB (y-axis). Fold increase calculated from increase in bulk membrane localization kinetics of Dy647-PI3Kβ showing single molecule displacements from > 500 Dy647-PI3Kβ particles (>10,000 steps) measured on SLBs at pY surface densities of 0µM, 10µM, 20µM, and 30µM. (C) Single molecule dwell time distributions measured in the presence of 10µM pY, 20µM pY, and 30µM pY. (D) Bulk membrane recruitment dynamics of 10 nM Dy647-PI3Kβ measured in the presence of pY alone or pY-Rac1(GTP). (E) Step size distributions showing single molecule displacements from > 500 Dy647-PI3Kβ particles (>10,000 steps) in the presence of either pY alone or pY-Rac1(GTP). (F) Bulk membrane recruitment dynamics of 10 nM Dy647-PI3Kβ measured in the presence of either pY alone, pY-GβGγ, or pY(solution)-GβGγ. pY(solution) = 10 µM. (G) Step size distributions showing single molecule displacements from > 500 Dy647-PI3Kβ particles (>10,000 steps) in the presence of either pY alone or pY-GβGγ. Membrane composition: 96% DOPC, 2% PI(4,5)P_2, 2% MCC-PE.

Active Rac1 and GβGγ work synergistically with pY to activate PI3Kβ.

To show the distinct difference between Rac1 working to localize and activate PI3Kβ, we designed an experiment to separate these two activities. This dual measurement experiment measures both the localization of Dy647-PI3Kβ and the activation of PI3Kβ by measuring production of $PI(3,4,5)P_3$ using the Btk sensor we have purified and tested. In order for PI3Kβ to perform its catalytic activity of converting $PI(4,5)P_2$ to $PI(3,4,5)P_3$, ATP must be present to donate a phosphate for phosphorylation of the 3' position of the inositol ring of $PI(4,5)P_2$. For the first 5 minutes after Dy647-PI3Kβ is added to the tethered Rac1 containing bilayer, there will be no ATP present, so we expect to see little to no production of $PI(3,4,5)P_3$, but we do expect to see localization of Dy647-PI3Kβ at the membrane. After 5 minutes the ATP is added, and if the Rac1 is activating the Dy647-PI3Kβ, we expect to see a jump in production of $PI(3,4,5)P_3$, but little to no additional localization. In the first experiment, we are using the inactive, GDP bound, form of Rac1. This inactive form shows some localization and activation during the first five minutes, but when ATP is added and catalysis begins, we see a small increase in localization and a gradual increase in $PI(3,4,5)P_3$ production over the following 20 minutes (**Figure 6A**). In the second experiment, we see a similarly low level of activation during the first 5 minutes, but greater localization by the active, GTP bound, Rac1. This confirms that active Rac1 and tethered pY peptides are synergistically localizing Dy647-PI3Kβ, but as we expected, without ATP they are unable to activate Dy647-PI3Kβ. After ATP is added, we see a small jump in localization of Dy647-PI3Kβ and a fast increase in production of $PI(3,4,5)P_3$ (**Figure 6A**). Collectively these data tell us that tethered pY peptides and Rac1 in its GTP bound form synergistically activate Dy647-PI3Kβ, leading to production of $PI(3,4,5)P_3$.

The Btk biosensor was also used to measure the activation of PI3Kβ by GβGγ using a single biosensor experiment to measure the production of $PI(3,4,5)P_3$ lipids. At a 2nM concentration, tethered pY peptides are able to activate production of $PI(3,4,5)P_3$ lipids, without any additional small molecules. When GβGγ is passively absorbed into the supported membrane along with the tethered pY peptides, only a 20pM concentration of PI3Kβ is needed to see the same levels of production of $PI(3,4,5)P_3$ lipids, 100 times lower of a concentration. Using the same low concentration of PI3Kβ and pY peptides, almost no $PI(3,4,5)P_3$ production can be seen (**Figure 6B**). This data confirms our hypothesis that GβGγ and pY peptides synergistically activate PI3Kβ, highlighting the important role GβGγ plays in activation.

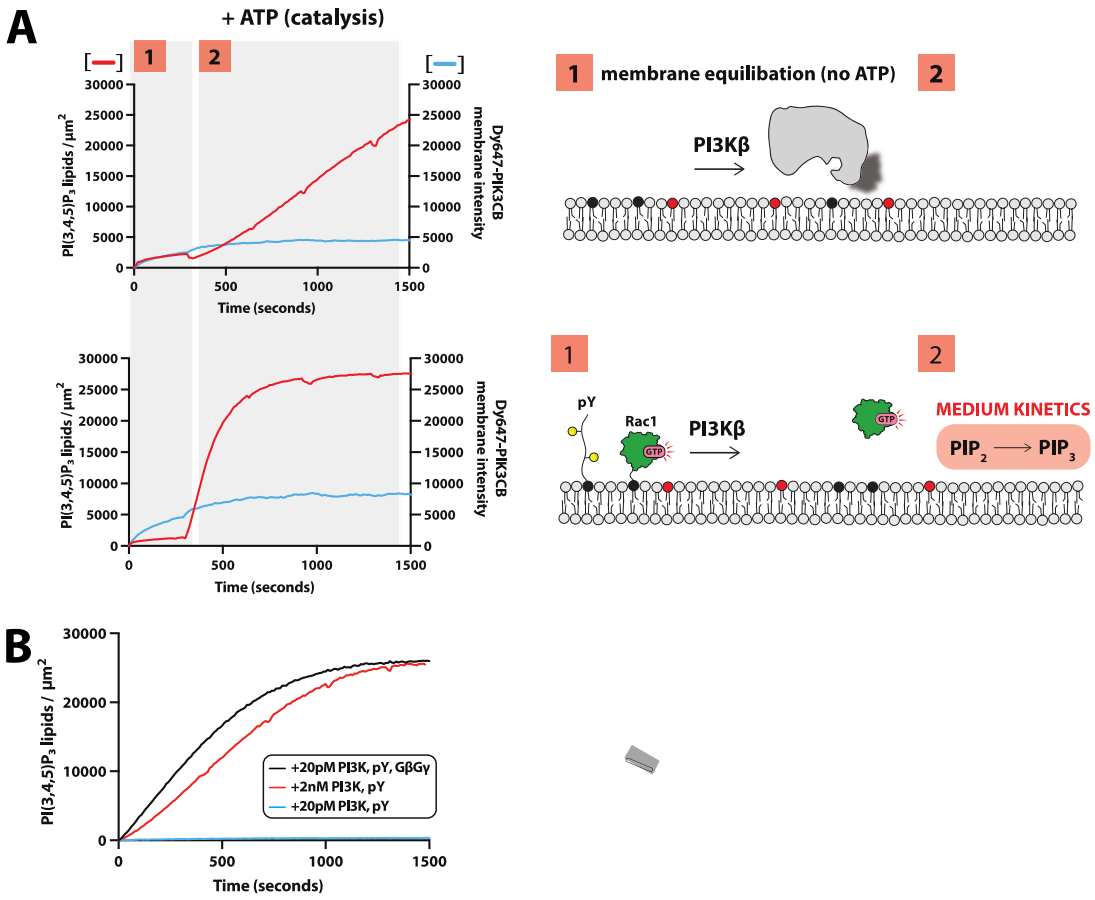

Figure 6. Active Rac1 and GβGγ work synergistically with pY to activate PI3Kβ.

(A) Dual color TIRF-M imaging showing 2 nM Dy647-PI3Kβ localization and catalysis measured in the presence of 20nM Btk-SNAP-Ax488, and cartoon schematic illustrating method for measuring Dy647-PI3Kβ activity in the presence of either pY-Rac1(GDP) or pY-Rac1(GTP). Phase 1 of the reconstitution involves membrane equilibration of Dy647-PI3Kβ in the absence of ATP. During phase 2, 1 mM ATP is added to stimulate lipid kinase activity of Dy647-PI3Kβ. (B) Kinetics of $PI(3,4,5)P_3$ production monitored in the presence of 20nM Btk-Ax488 and either 20 pM or 2nM Dy647-PI3Kβ, and cartoon schematic illustrating method for measuring Dy647-PI3Kβ activity in the presence of either pY- GβGγ. Membrane contained either pY or pY-GβGγ. Membrane composition: 96% DOPC, 2% $PI(4,5)P_2$, 2% MCC-PE.

PI3Kα localization is mediated by pY peptides and HRas.

For our remaining paralog, PI3Kα, the literature has shown pY peptides and HRas GTPase to be involved in activity (Lee, 2011, Buckles, 2017). Just as in the PI3Kα experiments,

we used a combination of bulk and single molecule TIRF-M visualization studies to test their roles individually as well as synergistically in the activity of PI3Kα.

Similarly to PI3Kβ, we see no binding events in both the no input and pY in solution still images of Dy647-PI3Kα at a single molecule concentration regime, while when the pY is tethered with maleimide reactive lipids, we see some binding events of Dy647-PI3Kα (**Figure 7A**). We conclude from this data that membrane bound pY is also able to localize Dy647-PI3Kα and recruits more Dy647-PI3Kα than pY in solution does.

We hypothesized that this recruitment by pY of PI3Kα to the membrane would be similarly concentration dependent to PI3Kα. Following this hypothesis, we saw as the concentration of pY peptide tethered to the membrane was increased, a resulting linear increase in the density of membrane bound Dy647-PI3Kα could be seen (**Figure 7B**), telling us that this recruitment also has a positive correlation to pY peptide concentration. We also see similar step size diffusion population distributions for Dy647-PI3Kα measured across multiple pY membrane surface densities (**Figure 7C**), allowing us to conclude that this concentration dependent increase in localization is due to more PI3Kα molecules singly binding pY peptides at the membrane.

To measure the localization of PI3Kα by the small molecule GTPase HRas, we membrane tethered recombinantly purified HRas to the membrane using the same process as the pY peptides and Rac1. The pY peptides alone show localization of Dy647-PI3Kα without the addition of more small molecules, but after the addition of small GTPase HRas, we see a three-fold increase in the membrane intensity of Dy647-PI3Kα (**Figure 7D**), showing synergistic

localization by these two small molecules. The difference in the we see in the dwell times of Dy647-PI3Kα between these two experiments (**Figure 7E**) tells us that the increase in localization is due to Dy647-PI3Kα binding both pY peptides and HRas, keeping the molecules tethered to the membrane for longer periods of time.

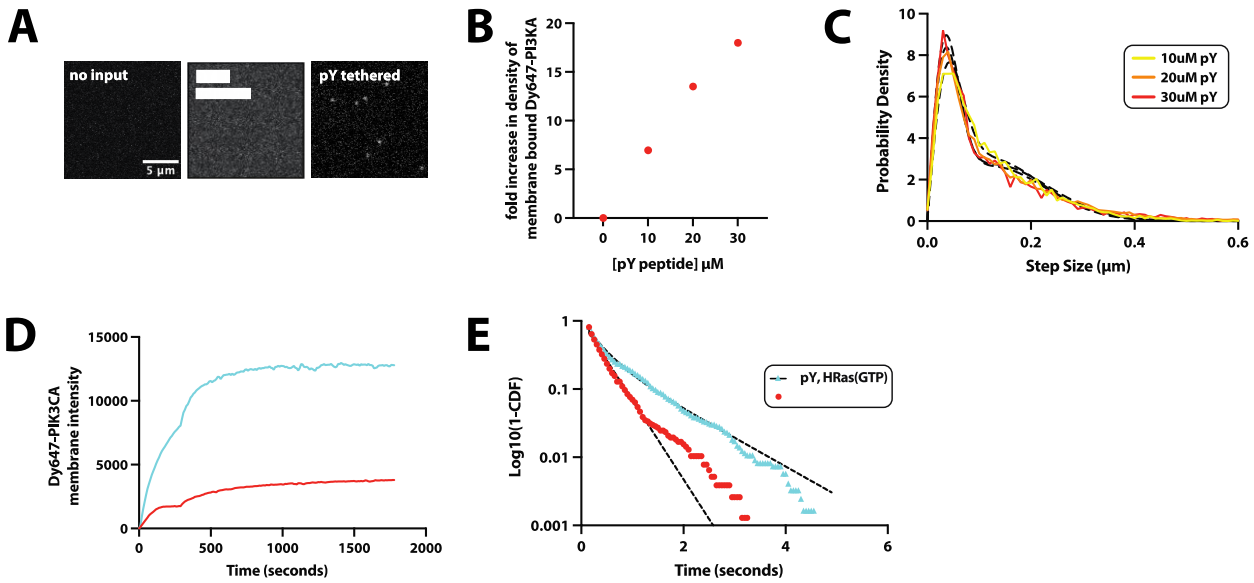

Figure 7. PI3Kα localization is mediated by pY peptides and HRas.

(A) Representative TIRF-M images showing the membrane localization of 5-10 pM Dy647-PI3Kα on membranes containing either no inputs, pY(solution), or pY(tethered). Supported membrane for pY tethered was conjugated with 10 µM pY peptide before adding Dy647-PI3Kα. pY(solution) = 10 µM. (B) Relationship between the total pY solution concentration (x-axis) used for covalent conjugation and the fold increase in density of membrane bound Dy647-PI3Kα (y-axis). Fold increase calculated from increase in bulk membrane localization kinetics of Dy647-PI3Kα showing single molecule displacements from > 500 Dy647-PI3Kα particles (>10,000 steps) measured on SLBs at pY surface densities of 0µM, 10µM, 20µM, and 30µM. (C) Single molecule dwell time distributions measured in the presence of 10µM pY, 20µM pY, and 30µM pY. (D) Bulk membrane recruitment dynamics of 10 nM Dy647-PI3Kα measured in the presence of pY alone or pY-HRas(GTP). (E) Step size distributions showing single molecule displacements from > 500 Dy647-PI3Kα particles (>10,000 steps) in the presence of either pY alone or pY-HRas(GTP). Membrane composition: 96% DOPC, 2% PI(4,5)P_2, 2% MCC-PE.

Active HRas works synergistically with pY to activate PI3Kα.

To measure the activation of PI3Kα by HRas, we used the Btk biosensor to measure the production of PI(3,4,5)P_3 lipids. Using the same maleimide reactive cysteine lipid tethers used to tether pY, HRas was tethered to the membrane. When pY alone is tethered to the membrane we see production of PI(3,4,5)P_3 lipids without the addition of any other small molecules (**Figure 8**),

suggesting that pY on its own is able to activate PI3Kα. The addition of inactive, GDP bound, HRas lead to a small increase in PI(3,4,5)P_3 production of about 2000 lipids per micron squared, but the rate of production remains slow. However, when we tether active, GTP bound, HRas, we see much faster production and an almost two-fold increase in PI(3,4,5)P_3 production for the just pY experiment (**Figure 8**). This suggests that active HRas and pY peptides synergistically activate PI3Kα. The increase that we see when HRas(GDP) is added to the membrane suggests to us that HRas is able to activate PI3Kα at some level in its GDP bound form, but this binding is not nearly as efficient as in the HRas GTP bound form.

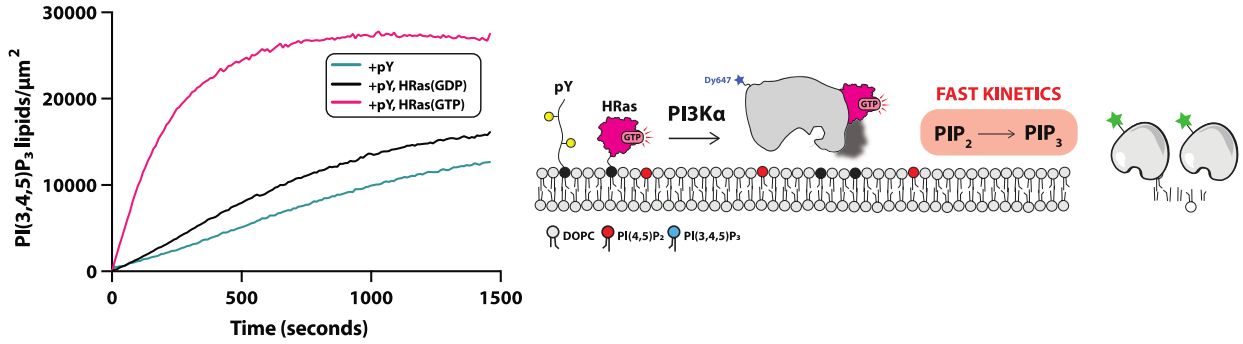

Figure 8. Active HRas works synergistically with pY to activate PI3Kα.

Kinetics of PI(3,4,5)P_3 production monitored in the presence of 20nM Btk-Ax488 and 2nM Dy647-PI3Kα, and cartoon schematic illustrating method for measuring Dy647-PI3Kβ activity in the presence of pY-HRas(GTP). Membrane contained either pY, pY-HRas(GDP), or pY-HRas(GTP). Membrane composition: 96% DOPC, 2% PI(4,5)P_2, 2% MCC-PE.

Discussion

Previous research into the effects of inputs on PI3K activity haven been done using solution-based assays, preventing researchers from directly visualizing signaling inputs. While these experiments were vital for identifying which inputs activate PI3K, they were unable to discern how these inputs localize the primarily cytoplasmic PI3K to the plasma membrane following receptor activation. Our TIRF-M experiments, coupled with anchoring the inputs in physiologically relevant conformations, allowed us to visualize the effect that molecular inputs had on PI3Kα and β localization and activation.

In order to accurately and reproducibly analyze production of $PI(3,4,5)P_3$ production, we first designed and tested the Btk biosensor as an alternative to the previously used Grp1 lipid sensor. We determined that Btk did not share the sensor accumulation issue that we had experienced with Grp1 when the Btk sensor plateaued at its maximum fluorescence intensity and did not continue to increase after reaction completion. Btk was shown to bind $PI(3,4,5)P_3$ by the same single binding pocket mechanism to Grp1 due to their similar population distributions of their step size diffusions. When designing efficient biosensors, we are searching for sensors that bind our molecules of interest specifically as well as bind quickly and leave quickly, so as to not interfere with any other binding events that may be occurring on the membrane. Following this criteria, Btk has a shorter dwell time and faster on rate (k_{on}) than Grp1, allowing us to conclude that Btk is a more efficient biosensor for measuring $PI(3,4,5)P_3$ lipid production.

The importance of pY peptides in the activation of PI3K has long been hypothesized, but in this study, we aimed to show the impacts of tethering phosphorylated tyrosines to the plasma

membrane. This membrane tethering has allowed us to reproduce a real cell environment *in vitro* more accurately, as pY peptides are derived from membrane tethered proteins such as RTKs. While it has been hypothesized that pY peptides in solution are able to bind to PI3K and disrupt its autoinhibition, these peptides floating in solution lack the ability to localize PI3K to the membrane. As we hypothesized, membrane tethered pY showed an increase in localization events at a single molecule regime of both PI3Kα and β over pY in solution. Based on our bulk recruitment data, membrane recruitment by pY peptides of PI3Kα and β is concentration dependent. The membrane diffusivity of PI3K at varying concentrations of pY peptides was indistinguishable, suggesting that each of these PI3K paralogs can bind only one pY peptide, given the strong correlation between diffusivity of tethered membrane proteins and valency of membrane interactions (Ziemba and Falke, 2013; Hansen, 2022).

Small GTPases Rac1 and HRas are unable to recruit their PI3K paralog without the presence of pY. Once bound to pY, however, we have shown that Rac1 and HRas can both enhance activation of PI3K, supporting the hypothesis of an autoinhibited PI3K (Rodriguez-Viciana, 1996; Yu, 1998). Based on our bulk activity measurements of PI3K, HRas and Rac1 GTPases in their active form increase localization of PI3Kα and β, respectively, in the presence of membrane tethered pY. The increase in PI3Kα localization by HRas is greater, about a 3-fold increase, than the 0.3-fold increase in PI3Kβ's localization by Rac1. We attribute the decrease in membrane diffusivity that we see when Rac1 is added to a membrane containing tethered pY peptides to PI3Kβ being doubly bound, once by pY and once by Rac1, at the membrane. A similar result can be seen in the increase in PI3Kα dwell time on a tethered pY membrane, where the addition of HRas leads PI3Kα to remain at the membrane for a longer period of time. A

doubly bound PI3K protein would have less freedom of movement across the membrane, leading it to show lower diffusivity and dwell time.

The activity of PI3Kβ has been shown to be increased by another small molecule, GβGγ, but only in the presence of pY peptides (Maier, 2000). In line with these results, our bulk localization study shows that tethered pY and GβGγ synergistically localize PI3Kβ at a two-fold higher level than tethered pY alone. However, when GβGγ is present on the membrane and pY peptides are only present in solution, GβGγ is unable to recruit PI3Kβ to the membrane. Additionally, the decrease in membrane diffusivity of PI3Kβ when both tethered pY and GβGγ are present suggests a similar doubly bound mechanism of PI3Kβ localization, where it binds to one GβGγ and one pY peptide.

Building on our localization findings, we also show that GTPases Rac1 and HRas are involved in the activation of their PI3K paralogs, catalyzing the conversion of $PI(4,5)P_2$ lipids to $PI(3,4,5)P_3$ lipids. Based on the results of our dual measurement experiment for PI3Kβ, Rac1(GDP) displays slow kinetics, while when it switches conformations to Rac1(GTP), it displays fast kinetics. Since Rac1(GTP) is its active conformation, we would expect it to show this more effective activation of PI3Kβ than in its inactive conformation. However, our data does suggest that even Rac1(GDP) is still able to bind and activate PI3Kβ, just at a slower rate. Similarly, HRas(GDP) displays slow reaction kinetics, reaching only about half the total lipids produced by HRas(GTP) over the given time period. The production of $PI(3,4,5)P_3$ by HRas(GTP) is much more rapid, displaying fast kinetics, and reaches its maximum lipid production in about half the time needed by its inactive form. Addition of GβGγ shows

additional synergistic activation of PI3Kβ when combined with tethered pY. Together these two molecules activate 20pM PI3Kβ at the same activity level as a much more highly concentrated 2nM PI3Kβ sample that only has tethered pY peptides present. When GTPases in their active forms or GβGγ are added to a pY tethered membrane, the resulting change in PI3K activation seen is significantly greater than the change in PI3K localization that these molecules show. This result suggests to us that the activation of both PI3Kα and β are allosterically modulated, improving PI3K's catalytic efficiency.

The activities of PI3K paralogs α and β are controlled by a highly regulated pathways involving a combination of synergistic localization and activation by a number of small molecules. Our results visualize the novel finding that in both PI3Kα and β, initial binding by RTK derived phosphorylated tyrosine residues is the primary driving step in localization. After relieving the autoinhibition through this binding of pY peptides, PI3K undergoes an allosteric change in conformation, allowing PI3Kα to bind the small GTPase HRas, and PI3Kβ to bind the small GTPase Rac1 or the heterotrimeric G-proteins, GβGγ. Binding by these two proteins shows synergistic membrane localization, but most importantly dramatic synergistic activation of PI3K.

Methods

Cloning and purification of Btk construct.

The Btk PH domain protein construct used in our research was supplied by the Jean Chung lab at Colorado State University. This construct contained a C-terminal EGFP tag, which was removed and replaced with a SNAP tag using standard molecular cloning procedures. The coding sequence of the new his6-SUMO-Btk(PH-TH)-RKSS-SNAP was expressed in BL21 Star *E. coli* bacteria were grown at 37°C in Terrific Broth to an OD600 of 0.8. These cultures were then shifted to 18°C for 1 hr, induced with 0.1 mM IPTG, and allowed to express protein for 20 hr at 18°C before being harvested. Cells were lysed into 50 mM Na_3PO_4 (pH 8.0), 400 mM NaCl, 0.5 mM BME, 10 mM Imidazole, and 5% glycerol. Lysate was then centrifuged at 16,000 rpm (35,172 × g) for 60 min in a Beckman JA-17 rotor chilled to 4°C. Lysate was circulated over 5 mL HiTrap Chelating column (GE Healthcare, Cat# 17-0409-01) charged with 100 mM CoCl2 for 1 hr. Bound protein was then eluted with a linear gradient of imidazole (0–500 mM, 8 CV, 40 mL total, 2 mL/min flow rate). Peak fractions were pooled, combined with SUMO protease Ulp1 (50 µg/mL final concentration), and dialyzed against 4 L of buffer containing 20 mM Tris (pH 7.0), 200 mM NaCl, and 0.5 mM BME for 16–18 hr at 4°C. Dialysate-containing SUMO cleaved protein was recirculated for 1 hr over a 5 mL HiTrap Chelating column. Flow-through containing Btk-SNAP was then concentrated in a 5 kDa MWCO Vivaspin 20 before being loaded on a Superdex 75 size-exclusion column equilibrated in 20 mM Tris (pH 7.0), 200 mM NaCl, 10% glycerol, 1 mM TCEP. Peak fractions containing Btk-SNAP were pooled and concentrated to a concentration of 30 µM before snap-freezing with liquid nitrogen and storage at –80°C. For labeling, Btk-SNAP was combined with a 1.5x molar excess of SNAP-Surface Alexa488 dye (NEB, Cat# S9129S) and incubated overnight at 4ºC. The next day, Btk-SNAP-AF488 was

desalted into buffer containing 20 mM Tris [pH 8.0], 200 mM NaCl, 10% glycerol, 1 mM TCEP using a PD10 column. The protein was then spin concentrated using a Amicon filter and loaded onto a Superdex 75 column to isolate dye free monodispersed Btk-SNAP-AF488. The peak elution was pooled, concentrated, aliquoted, and flash frozen with liquid nitrogen.

Preparation of supported lipid bilayers.

We generated small unilamellar vesicles (SUVs) for this study using the following lipids: 1,2-dioleoyl-sn-glycero-3-phosphocholine (18:1 DOPC, Avanti # 850375C) and 1,2-dioleoyl-sn-glycero-3-phospho-L-serine (18:1 DOPS, Avanti # 840035C), L-α-phosphatidylinositol-4,5-bisphosphate (Brain PI(4,5)P_2, Avanti # 840046X), and 1,2-dioleoyl-sn-glycero-3-phosphoethanolamine-N-[4-(p-maleimidomethyl)cyclohexane-carboxamide] (18:1 MCC-PE, Avanti # 780201C). We report lipid mixtures as percentages equivalent to molar fractions.

We dried a total of 2 μmoles lipids and combined with 2 mL of chloroform in a 35 mL glass round bottom flask. This mixture was dried to a thin film via rotary evaporation where the glass round-bottom flask was kept in a 42ºC water bath. Following evaporation, we placed the lipid-containing flask in a vacuum desiccator for a minimum of 30 minutes. We obtained a concentration of 1 mM of lipids by resuspending the dried film in 2 mL of 1x PBS [pH 7.2] We generated 30-50 nm SUVs from this 1 mM total lipid mixture via extrusion of the resuspended lipid mixture through 0.03 μm pore size 19 mm polycarbonate membrane (Avanti #610002) with filter supports (Avanti #610014) on both sides of the PC membrane.

We prepared coverglass (25x75 mm, IBIDI, cat #10812) for depositing of SUV's by first cleaning with heated (60-700C) 2% Hellmanex III (Fisher, Cat#14-385-864) in a glass coplin jar. We incubated hot Hellmanex III and coverglass for at least 30 minutes before rinsing with

MilliQ water. The cleaned glass was then etched with Piranha solution (1:3, hydrogen peroxide:sulfuric acid) for 10-15 minutes. We rinsed and stored the etched coverglass in MilliQ, then rapidly dried our MilliQ-rinsed etched coverglass slides with nitrogen gas before adhering to a 6-well sticky-side chamber (IBIDI, Cat# 80608). SLBs were created by flowing 100-150 µL of SUVs with a total lipid concentration of 0.25 mM in 1x PBS [pH 7.2] into the IBIDI chamber. Following 30 minutes of incubation, supported membranes were washed with 4 mL of 1x PBS [pH 7.2] to remove non-absorbed SUVs. To block membrane defects, we prepared 1 mg/mL beta casein (Thermo FisherSci, Cat# 37528) by clarifying with a centrifugation step at 4°C for 30 minutes at 21370 x g before passing through 0.22 µm syringe filtration unit (0.22 µm PES syringe filter (Foxx Life Sciences, Cat#381-2116-OEM)). We then blocked membrane defects with 1 mg/mL beta casein (Thermo FisherSci, Cat# 37528) for 5-10 minutes.

Protein conjugation of maleimide lipid.

After blocking SLBs with beta casein, membranes were washed with 2 mL of 1x PBS and stored at room temperature for up to 2 hours before mounting on the TIRF microscope. Prior to single molecule imaging experiments, supported membranes were washed into TIRF imaging buffer. Supported membrane containing with MCC-PE lipids were used to covalently couple either HRas(GDP) or phosphotyrosine peptide (pY). For these SLBs, 100 µL of 30 µM HRas diluted in a 1x PBS [pH 7.2] and 0.1 mM TCEP buffer was added to the IBIDI chamber and incubated for 2 hours at 23ºC. The addition of TCEP significantly increases the coupling efficiency. SLBs with MCC-PE lipids were then washed with 2 mL of 1x PBS [pH 7.2] containing 5 mM betamercaptoethanol (BME) and incubated for 15 minutes to neutralize the

unreacted maleimide headgroups. SLBs were washed with 1 mL of 1x PBS, followed by 1 mL of kinase buffer before starting TIRF-M experiments.

Activation of Rac1/HRas on supported lipid bilayer.

Membrane conjugated Rac1(GDP) was converted to Rac1(GTP) using either chemical activation (i.e. EDTA/GTP/$MgCl_2$) or with a guanine nucleotide exchange factor (GEF). Chemical activation was achieved by first washing supported membranes containing maleimide conjugated Rac1(GDP) with buffer containing 1x PBS, 1 mM EDTA, 1 mM GTP. This was followed by a 15-minute incubation to exchange GDP for GTP. To stably associate the newly loaded GTP with Rac1, chambers containing the SLBs were subsequently washed with 1x PBS, 1 mM $MgCl_2$, 50 μM GTP. A complementary approach that utilizes GEF-mediated activation of Rac1 was achieved by flowing 50 nM P-Rex1 DH-PH domain over Rac1(GDP) conjugated membranes. The mechanism of activation was carried out in buffer containing 1x PBS, 1 mM $MgCl_2$, 50 μM GTP. Both methods of activation yielded the same density of Rac(GTP) and have been validated in previous studies. The same methods can be used in the activation of HRas, replacing the GEF P-Rex1 with Soscat.

Single molecule TIRF microscopy.

We performed all supported membrane TIRF-M experiments in buffer containing 20 mM HEPES [pH 7.0], 150 mM NaCl, 1 mM ATP, 5 mM $MgCl_2$, 0.5 mM EGTA, 20 mM glucose, 200 μg/mL beta casein (ThermoScientific, Cat# 37528), 20 mM BME, 320 μg/mL glucose oxidase (Biophoretics, Cat #B01357.02 *Aspergillus niger*), 50 μg/mL catalase (Sigma, #C40-

100MG Bovine Liver), and 2 mM Trolox (Cayman Chemicals, Cat#). Perishable reagents (i.e. glucose oxidase, catalase, and Trolox) were added 5-10 minutes before image acquisition.

Microscope hardware and imaging acquisition.

Single molecule imaging experiments were performed at room temperature (23ºC) using an inverted Nikon Ti2 microscope using a 100x oil immersion Nikon TIRF objective (1.49 NA). We controlled the x-axis and y-axis position using a Nikon motorized stage, joystick, and Nikon's NIS element software. We also controlled microscope hardware using Nikon NIS elements. Fluorescently labelled proteins were excited with one of three diode lasers: a 488 nm, 561nm, or 637 nm (OBIS laser diode, Coherent Inc. Santa Clara, CA). The lasers were controlled with a Vortran laser launch and acousto-optic tuneable filters (AOTF) control. Excitation and emission light was transmitted through a multi-bandpass quad filter cube (C-TIRF ULTRA HI S/N QUAD 405/488/561/638; Semrock) containing a dichroic mirror. The laser power measured through the objective for single particle visualized was 1-3 mW. Fluorescence emission was captured on an iXion Life 897 EMCCD camera (Andor Technology Ltd., UK) after passing through one of the following 25 mm Nikon Ti2 emission filters mounted in a Nikon emission filter wheel: ET525/50M, ET600/50M, and ET700/75M (Semrock).

Kinetics measurements of PI(3,4,5)P_3 lipid production.

The phosphorylation of PI(3,4,5)P_3 was measured on SLB's formed in IBIDI chambers visualized via TIRF microscopy. We monitored the production of PI(3,4,5)P_3 produced by solution-based PI3K at the membrane surface using solution concentrations of 50 nM Alex555-Grp1 or 50 nM Alexa488-Btk. Reaction buffer for experiments contained 20mM HEPES (pH

7.0), 150 mM NaCl, 5 mM $MgCl_2$, 1 mM ATP, 0.1mM GTP, 0.5 mM EGTA, 20 mM glucose, 200 μg/mL beta casein (Thermo Scientific, Cat# 37528), 20 mM BME, 320 μg/mL glucose oxidase (Serva, #22780.01 Aspergillus *niger*), 50 μg/mL catalase (Sigma, #C40-100MG Bovine Liver), and 2 mM Trolox (UV treated, 15-90 minutes; REF). In experiments where inactive GTPases were coupled to membranes, no ATP was present in the reaction buffer and the 0.1 mM of GTP was replaced with 0.1 mM of GDP. Perishable reagents were added 5-10 minutes before image acquisition.

Image processing, statistics, and data analysis.

Image analysis was performed on ImageJ/Fiji and MatLab. Curve fitting was performed using Prism 9 (GraphPad).

Single particle tracking.

Single fluorescent Dy647-PI3Kβ/α complexes bound to supported lipid bilayers were detected using the ImageJ/Fiji TrackMate plugin (Jaqaman et al. 2008). Data in the form of a .nd2 file was loaded in ImageJ/Fiji and the LoG detector was used to identify particles based on brightness and their signal-to-noise ratio. After locating every fluorescent particle, we used the LAP tracker to generate particle trajectories that followed molecular displacement over time. Particle trajectories were then filtered based on track start (remove particles at start of movie), track end (remove particles at end of movie), duration (particles track ≥ 2 frames), track displacement, and X - Y location (removed particles near the edge of the movie). The output files from TrackMate were then analyzed using custom MATLAB scripts to calculate the single molecule dwell time of membrane bound Dy647-PI3Kβ/α. To calculate the dwell times of

membrane bound proteins, we generated cumulative distribution frequency (CDF) plots with the bin size set to image acquisition frame interval (e.g. 52 ms). The $\log_{10}$(1-CDF) was plotted as a function dwell time and fit to a single or double exponential curve. For the double exponential curve fits, the alpha value is the percentage of the fast-dissociating molecules characterized by the time constant, τ_1. A typical data set contained dwell times measured for n = 1000 trajectories repeated as n = 3 technical replicates.

Single exponential model: $f(t) = e^{(-x/\tau)}$

Two exponential model: $f(t) = \alpha * e^{(-x/\tau 1)} + (1-\alpha) * e^{(-x/\tau 2)}$

To calculate the diffusion coefficient (μm^2/sec), we plotted probability density (i.e. frequency divided by bin size of 0.01 μm) versus step size (μm). The step size distribution was fit to the following models.

Single species model: $f(r) = \frac{r}{2D\tau} e^{-(\frac{r^2}{4D\tau})}$

Two species model: $f(r) = \alpha \frac{r}{2D_1\tau} e^{-(\frac{r^2}{4D_1\tau})} + (1-\alpha) \frac{r}{2D_2\tau} e^{-(\frac{r^2}{4D_2\tau})}$

Bibliography

Balla, Tamas. “Phosphoinositides: Tiny Lipids With Giant Impact on Cell Regulation.” Physiological Reviews, vol. 93, no. 3, July 2013, pp. 1019–137, https://doi.org/10.1152/physrev.00028.2012.

Baraldi, Elena, et al. “Structure of the PH Domain from Bruton’s Tyrosine Kinase in Complex with Inositol 1,3,4,5-Tetrakisphosphate.” Structure, vol. 7, no. 4, Apr. 1999, pp. 449–60, https://doi.org/10.1016/S0969-2126(99)80057-4.

Buckles, Thomas C., et al. “Single-Molecule Study Reveals How Receptor and Ras Synergistically Activate PI3Kα and PIP3 Signaling.” Biophysical Journal, vol. 113, no. 11, Dec. 2017, pp. 2396–405, https://doi.org/10.1016/j.bpj.2017.09.018.

Castellano, E., and J. Downward. “RAS Interaction with PI3K: More Than Just Another Effector Pathway.” Genes & Cancer, vol. 2, no. 3, Mar. 2011, pp. 261–74, https://doi.org/10.1177/1947601911408079.

Chung, Jean K., et al. “Switch-like Activation of Bruton’s Tyrosine Kinase by Membrane-Mediated Dimerization.” Proceedings of the National Academy of Sciences, vol. 116, no. 22, May 2019, pp. 10798–803, https://doi.org/10.1073/pnas.1819309116.

Cole, Nelson B. “Site-Specific Protein Labeling with SNAP-Tags.” Current Protocols in Protein Science, vol. 73, no. 1, Aug. 2013, https://doi.org/10.1002/0471140864.ps3001s73.

Dbouk, Hashem A., et al. “G Protein–Coupled Receptor–Mediated Activation of P110β by Gβγ Is Required for Cellular Transformation and Invasiveness.” Science Signaling, vol. 5, no. 253, Dec. 2012, https://doi.org/10.1126/scisignal.2003264.

Di Paolo, Gilbert, and Pietro De Camilli. “Phosphoinositides in Cell Regulation and Membrane Dynamics.” Nature, vol. 443, no. 7112, Oct. 2006, pp. 651–57, https://doi.org/10.1038/nature05185.

Erdmann, Roman S., et al. “Labeling Strategies Matter for Super-Resolution Microscopy: A Comparison between HaloTags and SNAP-Tags.” Cell Chemical Biology, vol. 26, no. 4, Apr. 2019, pp. 584-592.e6, https://doi.org/10.1016/j.chembiol.2019.01.003.

Fernández-Medarde, Alberto, et al. “Anthraquinones as Inhibitors of SOS RAS-GEF Activity.” Biomolecules, vol. 11, no. 8, July 2021, p. 1128, https://doi.org/10.3390/biom11081128.

Fox, Millie, et al. “Class IA PI3K Regulatory Subunits: P110-Independent Roles and Structures.” Biochemical Society Transactions, vol. 48, no. 4, Aug. 2020, pp. 1397–417, https://doi.org/10.1042/BST20190845.

Fritsch, Ralph, et al. “RAS and RHO Families of GTPases Directly Regulate Distinct Phosphoinositide 3-Kinase Isoforms.” Cell, vol. 153, no. 5, May 2013, pp. 1050–63, https://doi.org/10.1016/j.cell.2013.04.031.

Graziano, Brian R., et al. “A Module for Rac Temporal Signal Integration Revealed with Optogenetics.” Journal of Cell Biology, vol. 216, no. 8, Aug. 2017, pp. 2515–31, https://doi.org/10.1083/jcb.201604113.

Guillermet-Guibert, Julie, et al. “The P110ᴺʟ Isoform of Phosphoinositide 3-Kinase Signals Downstream of G Protein-Coupled Receptors and Is Functionally Redundant with P110.” Proceedings of the National Academy of Sciences of the United States of America, vol. 105, no. 24, June 2007, pp. 8292–97, https://doi.org/10.1073/pnas.0707761105.

Gymnopoulos, Marco, et al. “Rare Cancer-Specific Mutations in PIK3CA Show Gain of Function.” Proceedings of the National Academy of Sciences, vol. 104, no. 13, Mar. 2007, pp. 5569–74, https://doi.org/10.1073/pnas.0701005104.

Hall, Alan, et al. “Cellular Responses Regulated by Rho-Related Small GTP-Binding Proteins.” Philosophical Transactions of the Royal Society of London. Series B: Biological Sciences, vol. 340, no. 1293, June 1993, pp. 267–71, https://doi.org/10.1098/rstb.1993.0067.

Hamm, Heidi E. “The Many Faces of G Protein Signaling.” Journal of Biological Chemistry, vol. 273, no. 2, Jan. 1998, pp. 669–72, https://doi.org/10.1074/jbc.273.2.669.

Hammond, Gerald R., and Yang Hong. “Phosphoinositides and Membrane Targeting in Cell Polarity.” Cold Spring Harbor Perspectives in Biology, vol. 10, no. 2, Feb. 2018, p. a027938, https://doi.org/10.1101/cshperspect.a027938.

Hammond, Gerald R. V., et al. “PI4P and PI(4,5)P 2 Are Essential But Independent Lipid Determinants of Membrane Identity.” Science, vol. 337, no. 6095, Aug. 2012, pp. 727–30, https://doi.org/10.1126/science.1222483.

Hansen, Scott D., et al. “Membrane-Mediated Dimerization Potentiates PIP5K Lipid Kinase Activity.” ELife, vol. 11, Aug. 2022, p. e73747, https://doi.org/10.7554/eLife.73747.

He, Ju, et al. “Molecular Mechanism of Membrane Targeting by the GRP1 PH Domain*.” Journal of Lipid Research, vol. 49, no. 8, Aug. 2008, pp. 1807–15, https://doi.org/10.1194/jlr.M800150-JLR200.

Hendriks, Rudi W., et al. “Targeting Bruton’s Tyrosine Kinase in B Cell Malignancies.” Nature Reviews Cancer, vol. 14, no. 4, Apr. 2014, pp. 219–32, https://doi.org/10.1038/nrc3702.

Hoeller, Oliver, et al. “How to Understand and Outwit Adaptation.” Developmental Cell, vol. 28, no. 6, Mar. 2014, pp. 607–16, https://doi.org/10.1016/j.devcel.2014.03.009.

Hon, W. C., et al. “Regulation of Lipid Binding Underlies the Activation Mechanism of Class IA PI3-Kinases.” Oncogene, vol. 31, no. 32, Aug. 2012, pp. 3655–66, https://doi.org/10.1038/onc.2011.532.

Houslay, Daniel M., et al. “Coincident Signals from GPCRs and Receptor Tyrosine Kinases Are Uniquely Transduced by PI3Kβ in Myeloid Cells.” Science Signaling, vol. 9, no. 441, Aug. 2016, https://doi.org/10.1126/scisignal.aae0453.

Iijima, Miho, et al. “Temporal and Spatial Regulation of Chemotaxis.” Developmental Cell, vol. 3, no. 4, Oct. 2002, pp. 469–78, https://doi.org/10.1016/S1534-5807(02)00292-7.

Jean, Steve, and Amy A. Kiger. “Classes of Phosphoinositide 3-Kinases at a Glance.” Journal of Cell Science, vol. 127, no. 5, Mar. 2014, pp. 923–28, https://doi.org/10.1242/jcs.093773.

Ji, Tae H., et al. “G Protein-Coupled Receptors.” Journal of Biological Chemistry, vol. 273, no. 28, July 1998, pp. 17299–302, https://doi.org/10.1074/jbc.273.28.17299.

Jiménez, Concepción, Rosario Armas Portela, et al. “Role of the Pi3k Regulatory Subunit in the Control of Actin Organization and Cell Migration.” Journal of Cell Biology, vol. 151, no. 2, Oct. 2000, pp. 249–62, https://doi.org/10.1083/jcb.151.2.249.

Jiménez, Concepción, Carmen Hernández, et al. “The P85 Regulatory Subunit Controls Sequential Activation of Phosphoinositide 3-Kinase by Tyr Kinases and Ras.” Journal of Biological Chemistry, vol. 277, no. 44, Nov. 2002, pp. 41556–62, https://doi.org/10.1074/jbc.M205893200.

Kapeller, Rosana, and Lewis Cantley. “Phosphatidylinositol 3-Kinase.” BioEssays, vol. 16, no. 8, 1994, pp. 565–76, https://doi.org/10.1002/bies.950160810.

Lee, Jennifer Y., et al. “Inhibition of PI3K Binding to Activators by Serine Phosphorylation of PI3K Regulatory Subunit P85α Src Homology-2 Domains.” Proceedings of the National Academy of Sciences, vol. 108, no. 34, Aug. 2011, pp. 14157–62, https://doi.org/10.1073/pnas.1107747108.

Luo, Ji, et al. “The P85 Regulatory Subunit of Phosphoinositide 3-Kinase down-Regulates IRS-1 Signaling via the Formation of a Sequestration Complex.” Journal of Cell Biology, vol. 170, no. 3, Aug. 2005, pp. 455–64, https://doi.org/10.1083/jcb.200503088.

Maier, Udo, et al. “Gβ5γ2 Is a Highly Selective Activator of Phospholipid-Dependent Enzymes.” Journal of Biological Chemistry, vol. 275, no. 18, May 2000, pp. 13746–54, https://doi.org/10.1074/jbc.275.18.13746.

Marat, Andrea L., and Volker Haucke. “Phosphatidylinositol 3-phosphates—at the Interface between Cell Signalling and Membrane Traffic.” The EMBO Journal, vol. 35, no. 6, Mar. 2016, pp. 561–79, https://doi.org/10.15252/embj.201593564.

Nolte, R. T., et al. “Crystal Structure of the PI 3-Kinase P85 Amino-Terminal SH2 Domain and Its Phosphopeptide Complexes.” Nature Structural & Molecular Biology, vol. 3, no. 4, Apr. 1996, pp. 364–74, https://doi.org/10.1038/nsb0496-364.

Nussinov, Ruth, et al. “Autoinhibition Can Identify Rare Driver Mutations and Advise Pharmacology.” The FASEB Journal, vol. 34, no. 1, Jan. 2020, pp. 16–29, https://doi.org/10.1096/fj.201901341R.

Okkenhaug, Klaus. “Signaling by the Phosphoinositide 3-Kinase Family in Immune Cells.” Annual Review of Immunology, vol. 31, no. 1, Mar. 2013, pp. 675–704, https://doi.org/10.1146/annurev-immunol-032712-095946.

Olayioye, Monilola A., et al. “Spatiotemporal Control of Intracellular Membrane Trafficking by Rho GTPases.” Cells, vol. 8, no. 12, Nov. 2019, p. 1478, https://doi.org/10.3390/cells8121478.

Pilling, Carissa, et al. “The GRP1 PH Domain, Like the AKT1 PH Domain, Possesses a Sentry Glutamate Residue Essential for Specific Targeting to Plasma Membrane PI(3,4,5)P 3.” Biochemistry, vol. 50, no. 45, Nov. 2011, pp. 9845–56, https://doi.org/10.1021/bi2011306.

Rameh, Lucia E., et al. “Phosphatidylinositol (3,4,5)P3 Interacts with SH2 Domains and Modulates PI 3-Kinase Association with Tyrosine-Phosphorylated Proteins.” Cell, vol. 83, no. 5, Dec. 1995, pp. 821–30, https://doi.org/10.1016/0092-8674(95)90195-7.

Rathinaswamy, Manoj K., et al. “Structure of the Phosphoinositide 3-Kinase (PI3K) P110γ-P101 Complex Reveals Molecular Mechanism of GPCR Activation.” Science Advances, vol. 7, no. 35, Aug. 2021, p. eabj4282, https://doi.org/10.1126/sciadv.abj4282.

Rodriguez-Viciana, P., et al. “Activation of Phosphoinositide 3-Kinase by Interaction with Ras and by Point Mutation.” The EMBO Journal, vol. 15, no. 10, May 1996, pp. 2442–51, https://doi.org/10.1002/j.1460-2075.1996.tb00602.x.

Rodriguez-Viciana, Pablo, et al. “Phosphatidylinositoi-3-0H Kinase as a Direct Target of Ras.” Nature, vol. 370, no. 6490, Aug. 1994, pp. 527–32, https://doi.org/10.1038/370527a0.

Stephens, L. R. “Agonist-Stimulated Synthesis of Phosphatidylinositol(3,4,5)-Trisphosphate: A New Intracellular Signalling System?” Biochimica et Biophysica Acta, vol. 1179, no. 1, Oct. 1993, pp. 27–75, https://doi.org/10.1016/0167-4889(93)90072-w.

Stephens, L. R., et al. “Pathway of Phosphatidylinositol(3,4,5)-Trisphosphate Synthesis in Activated Neutrophils.” Nature, vol. 351, no. 6321, May 1991, pp. 33–39, https://doi.org/10.1038/351033a0.

Thomason, P. A., et al. “A G-Protein Beta Gamma-Subunit-Responsive Phosphoinositide 3-Kinase Activity in Human Platelet Cytosol.” Journal of Biological Chemistry, vol. 269, no. 24, June 1994, pp. 16525–28, https://doi.org/10.1016/S0021-9258(19)89418-8.

Vanhaesebroeck, Bart, Sally Leevers, et al. “Phosphoinositide 3-Kinases: A Conserved Family of Signal Transducers.” Trends in Biochemical Sciences, vol. 22, no. 7, pp. 267–72, https://doi.org/10.1016/S0968-0004(97)01061-X.

Vanhaesebroeck, Bart, Julie Guillermet-Guibert, et al. “The Emerging Mechanisms of Isoform-Specific PI3K Signalling.” Nature Reviews Molecular Cell Biology, vol. 11, no. 5, May 2010, pp. 329–41, https://doi.org/10.1038/nrm2882.

Welch, Heidi C. E., et al. “P-Rex1, a PtdIns(3,4,5)P3- and G␣-Regulated Guanine-Nucleotide Exchange Factor for Rac.” Cell, vol. 108, no. 6, Mar. 2002, pp. 809–21, https://doi.org/10.1016/s0092-8674(02)00663-3.

Welch, Heidi CE. “Regulation and Function of P-Rex Family Rac-GEFs.” Small GTPases, vol. 6, no. 2, Apr. 2015, pp. 49–70, https://doi.org/10.4161/21541248.2014.973770.

Whitman, Malcolm, et al. “Type I Phosphatidylinositol Kinase Makes a Novel Inositol Phospholipid, Phosphatidylinositol-3-Phosphate.” Nature, vol. 332, no. 6165, Apr. 1988, pp. 644–46, https://doi.org/10.1038/332644a0.

Worthylake, David K., et al. “Crystal Structure of Rac1 in Complex with the Guanine Nucleotide Exchange Region of Tiam1.” Nature, vol. 408, no. 6813, Dec. 2000, pp. 682–88, https://doi.org/10.1038/35047014.

Yang, Hee Won, et al. “Cooperative Activation of PI3K by Ras and Rho Family Small GTPases.” Molecular Cell, vol. 47, no. 2, July 2012, pp. 281–90, https://doi.org/10.1016/j.molcel.2012.05.007.

Yu, Jinghua, et al. “Regulation of the P85/P110α Phosphatidylinositol 3′-Kinase.” Journal of Biological Chemistry, vol. 273, no. 46, Nov. 1998, pp. 30199–203, https://doi.org/10.1074/jbc.273.46.30199.

Zhang, Xuxiao, et al. “Structure of Lipid Kinase P110β/P85β Elucidates an Unusual SH2-Domain-Mediated Inhibitory Mechanism.” Molecular Cell, vol. 41, no. 5, Mar. 2011, pp. 567–78, https://doi.org/10.1016/j.molcel.2011.01.026.

Ziemba, Brian P., and Joseph J. Falke. “Lateral Diffusion of Peripheral Membrane Proteins on Supported Lipid Bilayers Is Controlled by the Additive Frictional Drags of (1) Bound Lipids and (2) Protein Domains Penetrating into the Bilayer Hydrocarbon Core.” Chemistry and Physics of Lipids, vol. 172–173, July 2013, pp. 67–77, https://doi.org/10.1016/j.chemphyslip.2013.04.005.